White Light Parametric Instabilities in Plasmas

B. Brandão*
GoLP/Instituto de Plasmas e Fusão Nuclear, Instituto Superior Técnico, 1049-001 Lisboa, Portugal

Parametric instabilities are central in many problems in plasma physics, in particular in laser-plasma interactions. Standard approaches are either based on a plane wave description or an incoherent pump (random phase approximation). In reality, most systems show partial coherence, where incoherence is induced by fluctuations or external passive systems (such is the case of inertial confinement fusion, for example). In recent works, a generalized Wigner-Moyal statistical theory of radiation, or generalized photon kinetics (GPK), has been introduced. GPK is formally equivalent to the full wave equation, thus allowing for a detailed description of stimulated scattering processes driven by partially coherent light. We have applied GPK to obtain a general dispersion relation for Stimulated Brillouin Scattering (SBS) driven by a spatially stationary radiation field with arbitrary statistics, which is valid for all ranges of coherence of the pump field. The monochromatic limit has been recovered from our general result, reproducing the classic monochromatic dispersion relation. The general dispersion relation has been numerically further explored, allowing for a study of the growth rate of the instability as a simultaneous function of the bandwidth of the pump wave, the intensity of the incident field, and the wavenumber of the scattered wave. The growth rate of SBS can be reduced by 1/3 for a bandwidth of 0.3 nm, for typical NIF parameters. A detailed comparison of our results with previous models for Forward SBS and Stimulated Brillouin Backscattering is also presented, as well as a comparison of the analytical results with one-dimensional particle-in-cell simulations.

I. INTRODUCTION

Due to the increasing attention dedicated to nonlinear and collective effects, the study of parametric instabilities has recently become a mandatory concern, reaching many fields of science [1]-[4]. The most common approach to the problem uses a coherent wave description, but the externally induced incoherence or the only partial coherence of most systems render this method incomplete.

The use of the Wigner distribution has proven to be powerful in studying this kind of instabilties, as some major developments have been carried out in nonlinear optics. With a derivation of a statistical description of a partially incoherent electromagnetic wave propagating in a nonlinear medium [5], it became clear that a stabilization of the modulational instability is possible as a result of an effect similar to Landau damping and caused by random phase fluctuations of the propagating wave, which is equivalent to the broadening of the Wigner spectrum. In similar studies [6], [7], focusing on the onset of the transverse instability in nonlinear media in the presence of a partially incoherent light, the Wigner distribution was once more confirmed as a suitable approach. The faster progression in nonlinear optics is partially justified by the validity of the paraxial wave approximation, which justifies a forward propagating ansatz for the evolution of electromagnetic waves in dispersive nonlinear media. In plasma physics, this is clearly a limitation, as many critical aspects in ICF, fast ignition and several applications in laser-plasma and astrophysical scenarios demand a detailed analysis of backscattered radiation.

The inclusion of bandwidth or incoherence effects in laser driven parametric instabilities has also been studied extensively. The addition of small random deflections to the phase of a plane wave was shown to significantly suppress the three-wave decay instability [8], which was one of the first suggestions of the spoiling of the laser coherence as a mean to avoid its deleterious effects. The threshold values for some electrostatic instabilities can also be effectively increased either by applying a random amplitude modulation to the laser or by the inclusion of a finite bandwidth of the pump wave [9], [10]. A new method for the inclusion of finite bandwidth effects on parametric instabilities, allowing arbitrary fluctuations of any group velocity, has also been developed [11], [12]. As far as the Stimulated Raman Scattering instability is concerned, it became clear that, although it may seriously decollimate a coherent laser beam, laser bandwidth is an effective way to suppress the instability [13].

A statistical description of light can be achieved through the Wigner-Moyal formalism of quantum mechanics, which provides, in its original formulation, a one-mode description of systems ruled by Schrödinger-like equations. In order to address other processes apart from the direct forward scattering, a generalization of this Photon Kinetics theory (GPK) was recently developed by J. E. Santos *et al.* [15]. This new formulation is completely equivalent to the full Klein-Gordon equation and was readily employed to derive a general dispersion relation for stimulated Raman scattering driven by white light [16].

In this paper, we focus on the study of the analytical and numerical properties of another white light parametric instability occurring in a plasma, the stimulated Brillouin scattering (SBS), and check its consistency with previous models. The suppression of the growth rate of the instability as a result of the inclusion of bandwidth in the pump wave is qualitative and quantitatively verified for realistic NIF parameters. We also perform broadband simulations of white light driven parametric instabilities, describing the implementation of a new module of the OSIRIS 2.0 PIC code that allows for pump waves with nonzero bandwidth.

This paper is organized as follows. In section II , we employ GPK to derive a general dispersion relation for SBS driven by a spatially stationary field with arbitrary statistics. We perform a detailed analytical study of different regimes of SBS and compare it with classical references dealing with the monochromatic limit of the instability. The whole domain of unstable wave numbers is numerically explored for a wide range of bandwidth choices. In section III, we compare the results of the numerical solution of our complete dispersion relation with the ones provided by a previous model for broadband SBS. In section IV, we support the results presented in the previous sections with output from PIC simulations. After a detailed study of an appropriate scenario for the onset of SBS pumped by a standard plane wave, we discuss and describe an implementation of pump wave's bandwidth in OSIRIS 2.0 and perform simulations of broadband effects in parametric instabilities. Finally, in section V, we state the conclusions.

II. BROADBAND STIMULATED BRILLOUIN SCATTERING

In the following we use normalized units, where length is normalized to c/ω_{p0}, with c the velocity of light in vacuum and $\omega_{p0} = (4\pi e^2 n_{e0}/m_e c^2)^{1/2}$ the electron plasma frequency, time

*Electronic address: bruno.brandao@ist.utl.pt

to $1/\omega_{p0}$, mass and absolute charge to those of the electron, respectively, m_e and e, with $e > 0$. The plasma is modeled as an interpenetrating fluid of both electrons and ions, with n_{e0} and n_{i0} their equilibrium (zeroth order) particle densities, respectively. Densities are also normalized to the equilibrium electron density, so we have $n_{e0} = 1$ and $n_{i0} = 1/Z$, where Z is the electric charge of the ions in units of e. As detailed in Ref. [16], we use $\mathbf{a}_p(\mathbf{r},t) = 2^{-1/2}(\hat{z} + i\hat{y})a_0 \int d\mathbf{k} A(\mathbf{k}) \exp[i(\mathbf{k}.\mathbf{r} - (\mathbf{k}^2+1)^{1/2}t)]$ as the normalized vector potential of the circularly polarized pump field, $\mathbf{a}_p = e\mathbf{A}_p/m_e c^2$, where $(\mathbf{k}^2+1)^{1/2} \equiv \omega(\mathbf{k})$ is the monochromatic dispersion relation in a uniform plasma. We also allow for a stochastic component in the phase of the vector potential $A(\mathbf{k}) = \hat{A}(\mathbf{k})\exp[i\psi(\mathbf{r},t)]$ such that $\left\langle \mathbf{a}_p^*(\mathbf{r}+\mathbf{y}/2,t).\mathbf{a}_p(\mathbf{r}-\mathbf{y}/2)\right\rangle = a_0^2 m(\mathbf{y})$ is independent of $\mathbf{r}$ with $m(0) = 1$ and $|m(\mathbf{y})|$ is bounded between 0 and 1, which means that the field is spatially stationary. In this section, $\tilde{q}$ denotes the first-order component of a generic quantity q. Unless specifically stated, the same notation for the functions and their Fourier transforms is used, as the argument of such functions (either $(\mathbf{r},t)$ or $(\mathbf{k},\omega)$) avoids any confusion. To obtain a dispersion relation for SBS we must couple the typical plasma response to an independently derived driving term, obtained within the GPK framework.

A. Plasma response and driving term

Combining the continuity and force equations for each species and closing the system with an isothermal equation of state, we can readily present without more detail the plasma response to the propagation of a light wave $\mathbf{a}_p$, beating with its scattered component $\tilde{\mathbf{a}}$, to produce the ponderomotive force of the laser [1]

$$\left(\frac{\partial^2}{\partial t^2} - 2\tilde{\nu}\partial t - c_S^2\nabla^2\right)\tilde{n} = \frac{Z}{M}\nabla^2 \mathrm{Re}[\mathbf{a}_p.\tilde{\mathbf{a}}], \tag{1}$$

with $c_S \equiv \sqrt{\frac{Z\theta_e}{M}}$ being the ion-sound velocity, M the mass of the ions, θ_e the electron temperature and $\tilde{\nu}$ an integral operator whose Fourier transform is $\nu|\mathbf{k}_L|c_S$.

In [27] we perform an independent derivation of what we call the driving term, which describes the way how the incident radiation is affected by the propagation in our dispersive medium. Although this term is usually described through the wave equation for the vector potential [1], [24], the study of white light parametric instabilities is not possible with this approach. The driving term obtained within the framework of GPK is

$$W_{\mathrm{Re}[\mathbf{a}_p.\tilde{\mathbf{a}}]} = \frac{1}{2}\tilde{n}\left[\frac{\rho_0\left(\mathbf{k}+\frac{\mathbf{k}_L}{2}\right)}{D_s^-} + \frac{\rho_0\left(\mathbf{k}-\frac{\mathbf{k}_L}{2}\right)}{D_s^+}\right], \tag{2}$$

where $D_s^{\pm} = \omega_L^2 \mp \left[\mathbf{k}.\mathbf{k}_L - \omega_L\omega\left(\mathbf{k}\mp\frac{\mathbf{k}_L}{2}\right)\right]$ and ω_L ($\mathbf{k}_L$) represents the instability frequency (wave vector).

B. General dispersion relation for Stimulated Brillouin Scattering and classical monochromatic limit

Performing time and space Fourier transforms on the plasma response and driving term ($\partial t \to i\omega_L, \nabla_{\mathbf{r}} \to -i\mathbf{k}_L$) yields

$$\mathcal{F}[\tilde{n}] = \frac{Z}{M}\frac{k_L^2}{\omega_L^2 + 2i\nu\omega_L|\mathbf{k}_L|c_S - c_S^2\mathbf{k}_L^2}\mathcal{F}\left[\mathrm{Re}[\mathbf{a}_p.\tilde{\mathbf{a}}]\right], \tag{3}$$

$$\mathcal{F}\left[W_{\mathrm{Re}[\mathbf{a}_p.\tilde{\mathbf{a}}]}\right] = \frac{1}{2}\mathcal{F}[\tilde{n}]\left[\frac{\rho_0\left(\mathbf{k}+\frac{\mathbf{k}_L}{2}\right)}{D_s^-} + \frac{\rho_0\left(\mathbf{k}-\frac{\mathbf{k}_L}{2}\right)}{D_s^+}\right], \tag{4}$$

with $D_s^{\pm} = \omega_L^2 \mp \left[\mathbf{k}.\mathbf{k}_L - \omega_L\omega\left(\mathbf{k}\mp\frac{\mathbf{k}_L}{2}\right)\right]$ and $c_S \equiv \sqrt{\frac{Z\theta_e}{M}}$.

The general dispersion relation can be obtained using one of the properties of the Wigner function [17]-[20]

$$\int W_{f.g}d\mathbf{k} = f^*g \Rightarrow \int \frac{W_{\mathrm{Re}[\mathbf{a}_p.\tilde{\mathbf{a}}]}}{\mathrm{Re}\left[\mathbf{a}_p.\tilde{\mathbf{a}}\right]}d\mathbf{k} = 1$$

as

$$1 = \frac{\omega_{pi}^2}{2}\frac{\mathbf{k}_L^2}{\omega_L^2 + 2i\nu\omega_L|\mathbf{k}_L|c_S - c_S^2\mathbf{k}_L^2}\int\left[\frac{\rho_0\left(\mathbf{k}+\frac{\mathbf{k}_L}{2}\right)}{D_s^-} + \frac{\rho_0\left(\mathbf{k}-\frac{\mathbf{k}_L}{2}\right)}{D_s^+}\right]d\mathbf{k}, \tag{5}$$

with $\omega_{pi} = \sqrt{Z/M}$ being the ion plasma frequency in normalized units and f^* representing the complex conjugate of f.

By making an appropriate change of variables, our general dispersion relation can be written in a more compact way

$$1 = \frac{\omega_{pi}^2}{2}\frac{\mathbf{k}_L^2}{\omega_L^2 + 2i\nu\omega_L|\mathbf{k}_L|c_S - c_S^2\mathbf{k}_L^2}\int\rho_0(\mathbf{k})\left(\frac{1}{D^+} + \frac{1}{D^-}\right)d\mathbf{k}, \tag{6}$$

with $D^{\pm}(\mathbf{k}) = [\omega(\mathbf{k}) \pm \omega_L]^2 - (\mathbf{k} \pm \mathbf{k}_L)^2 - 1$, the main result of this section.

We first apply our general dispersion relation to the simplest and most commonly treated case of a pump plane wave of wave vector $\mathbf{k}_0$, which means that $\rho_0(\mathbf{k}) = a_0^2\delta(\mathbf{k}-\mathbf{k}_0)$. With the purpose of the following comparisons, we drop the Landau damping contribution. The dispersion relation then becomes

$$1 = \frac{\omega_{pi}^2}{2}\frac{\mathbf{k}_L^2}{\omega_L^2 - c_S^2\mathbf{k}_L^2}a_0^2\left\{\frac{1}{[\omega(\mathbf{k}_0)+\omega_L]^2 - (\mathbf{k}_0+\mathbf{k}_L)^2 - 1} + \right.$$
$$\left. + \frac{1}{[\omega(\mathbf{k}_0)-\omega_L]^2 - (\mathbf{k}_0-\mathbf{k}_L)^2 - 1}\right\}. \tag{7}$$

This result recovers that of Ref. [1], which studies the case of a pump wave $\mathbf{A}_L = \mathbf{A}_{L0}\cos(\mathbf{k}_0.\mathbf{r} - \omega_0 t)$, if we account for the difference in polarization and use $\omega_0 = \omega(\mathbf{k}_0)$. All the conclusions derived in Ref. [1], based on this dispersion relation, are then consistent with the predictions of GPK [15].

C. 1D water-bag zero-order photon distribution function

We now work with a different profile for the pump wave, represented by the one-dimensional water-bag zero-order distribution function,

$$\rho_0(\mathbf{k}) = \frac{a_0^2}{\sigma_1+\sigma_2}[\theta(k-k_0+\sigma_1) - \theta(k-k_0-\sigma_2)], \tag{8}$$

where $\theta(k)$ is the Heaviside function and σ_1 (σ_2) represents the sprectal bandwidth to the left (right) of the central wave number, k_0.

For this distribution function, the autocorrelation function of the random phase $\psi(x)$ satisfies

$$\left\langle \exp\left[-i\psi\left(x+\frac{y}{2}\right) + i\psi\left(x-\frac{y}{2}\right)\right]\right\rangle = e^{-iy\tilde{\sigma}}\frac{\sin(y\bar{\sigma})}{y\bar{\sigma}}, \tag{9}$$

where $\tilde{\sigma} \equiv (\sigma_2 - \sigma_1)/2$ and $\bar{\sigma} \equiv (\sigma_1+\sigma_2)/2$. The correlation length of this distribution is $\approx \pi/\sqrt{2}\bar{\sigma}$.

A simplified dispersion relation for the water-bag distribution function of Eq. (8) can be derived (details of this derivation are presented in the complete thesis document [27]), yielding

$$1=\frac{a_0^2\omega_{pi}^2}{8\bar{\sigma}}\frac{k_L}{\omega_L^2-c_S^2k_L^2}\left[\frac{k_L^2}{k_L^2-\omega_L^2}\log\left(\frac{D_1^-D_2^+}{D_1^+D_2^-}\right)+\right.$$

$$\left.+\frac{2\omega_Lk_L}{\sqrt{Q_0}}(\text{arctanh }b^+ + \text{arctanh }b^-)\right], \quad (10)$$

with $\omega_{0i}=\sqrt{[k_0+(-1)^i\sigma_i]^2+1}$, $D_i^{\pm}=\omega_L^2-k_L^2\pm 2[(k_0+(-1)^i\sigma_i)k_L-\omega_{0i}\omega_L]$, $Q_0=(k_L^2-\omega_L^2)(k_L^2-\omega_L^2+4)$, $Q^{\pm}=\prod_{i=1}^2[D_i^{\pm}+(k_L-\omega_L)(\omega_L\mp 2\omega_{0i})]$ and $b^{\pm}=2k_L^2(\omega_L+k_L)\sqrt{Q_0}(2\bar{\sigma}+\omega_{01}-\omega_{02})/\left[Q^0k_L^2-Q^{\pm}(\omega_L+k_L)^2\right]$.

We are interested in an expression for the maximum growth rate of the Brillouin instability. Analytical results can be obtained in the case where all the photons of the distribution travel in an underdense medium, which implies that $k_0+(-1)^i\sigma_i >> 1$. This also guarantees that $k_0>\sigma_1$, which assures that $\rho_0(k)$ represents a broadband source of forward propagating photons. From this condition, the approximations $\omega_{0i}\approx k_0+(-1)^i\sigma_i$ and $b^{\pm}\approx 0$ are also valid.

The dispersion relation (10) then becomes

$$1=\frac{a_0^2\omega_{pi}^2}{8\bar{\sigma}}\frac{k_L^3}{\omega_L^2-c_S^2k_L^2}\frac{1}{k_L^2-\omega_L^2}\left\{\ln\left[\frac{2(k_0-\sigma_1)+(\omega_L+k_L)}{2(k_0-\sigma_1)-(\omega_L+k_L)}\right]+\right.$$

$$\left.+\ln\left[\frac{2(k_0+\sigma_2)-(\omega_L+k_L)}{2(k_0+\sigma_2)+(\omega_L+k_L)}\right]\right\}. \quad (11)$$

The resonance condition for SBS can be expressed as $\omega_L\sim k_Lc_S$ [1]. Furthermore, the backscattering regime of stimulated Brillouin scattering (SBBS) is known to provide the highest growth rates [1], so we make one of the terms D_i^+ resonant (corresponding to the contribution of the downshifted photons of the distribution function). By making the D_1^+ term resonant ($D_1^+=0\Rightarrow k_{L_{SBBS}}^m\approx\frac{2}{c_S+1}(k_0-\sigma_1)$), we are considering the contribution of the photons of the lowest wave number, while with D_2^+ ($D_2^+=0\Rightarrow k_{L_{SBBS}}^M\approx\frac{2}{c_S+1}(k_0+\sigma_2)$) we are searching for those of the highest wave number. This means that k_L is of the order of k_0 and the range of unstable wave numbers is

$$k_L\in\left[\frac{2}{c_S+1}(k_0-\sigma_1),\frac{2}{c_S+1}(k_0+\sigma_2)\right]. \quad (12)$$

We consider the upper limit case (as we will later see, the growth rate of the instability is within the same order of magnitude for the whole range of unstable wave numbers) and we note that $\omega_L\sim k_Lc_S$ implies that both $\omega_L<<k_L$ and $\omega_L<<k_0$.

1. Weak field limit

To account for the instability, we now write $\omega=k_Lc_S+i\Gamma$, with Γ being the real growth rate of the instability and $|\Gamma|<<k_Lc_S$ (the weak field limit). The dispersion relation (11) can then be rewritten in the form $1=A\ln B$ and we consider each term individually,

$$A=\frac{a_0^2\omega_{pi}^2}{8\bar{\sigma}}\frac{k_L^3}{\omega_L^2-c_S^2k_L^2}\frac{1}{k_L^2-\omega_L^2}\approx\frac{a_0^2\omega_{pi}^2(k_0+\sigma_2)}{4i(\sigma_1+\sigma_2)\Gamma c_Sk_L}; \quad (13)$$

$$B=\frac{2(k_0-\sigma_1)+(\omega_L+k_L)}{2(k_0-\sigma_1)-(\omega_L+k_L)}\frac{2(k_0+\sigma_2)-(\omega_L+k_L)}{2(k_0+\sigma_2)+(\omega_L+k_L)}\approx$$

$$\approx\frac{2k_0-\sigma_1+\sigma_2}{2(\sigma_1+\sigma_2)+i\Gamma}\frac{i\Gamma}{2(k_0+\sigma_2)}. \quad (14)$$

We now take the imaginary part of the dispersion relation, working with a real Γ and using the fact that, for a complex $Z=\rho e^{i\theta}$, with real ρ and θ, $\ln Z=\ln\rho+i\theta$. We get

$$\Gamma c_Sk_L=\frac{a_0^2\omega_{pi}^2(k_0+\sigma_2)}{4(\sigma_1+\sigma_2)}\arctan\left[\frac{2(\sigma_1+\sigma_2)}{\Gamma}\right]. \quad (15)$$

With this result we are now able to compare our results for backscattering with those of [1]. We found $k_{L_{SBBS}}^m\approx\frac{2}{c_S+1}(k_0-\sigma_1)$ and $k_{L_{SBBS}}^M\approx\frac{2}{c_S+1}(k_0+\sigma_2)$, which implies that, for the monochromatic limit, $k_{L_{SBBS}}^{m,pw}=k_{L_{SBBS}}^{M,pw}\equiv k_{L_{SBBS}}^{pw}=\frac{2}{c_S+1}k_0\approx 2k_0(1-c_S)=2k_0-2\omega_0c_S$, because $\omega_0\equiv\omega_{01}(\sigma_1=0)=\omega_{02}(\sigma_2=0)\approx k_0$, where we have considered that the ion acoustic velocity is much smaller than the speed of light. This recovers the result of Ref. [1] for the wave number that maximizes the growth rate.

In what concerns to the maximum growth rate in the weak field (wf) scenario, we take the limit $\sigma_1,\sigma_2\to 0$ and make use of $\arctan x\sim x$ when $x\to 0$

$$\Gamma_{SBBSwf}^{pw,\max}=\frac{1}{2\sqrt{2}}\frac{k_0\sqrt{2}a_0\omega_{pi}}{\sqrt{\omega_0k_0c_S}}. \quad (16)$$

which also coincides with the monochromatic result in [1] if we consider the already discussed correction for the polarization.

We now go back to the general case of Eq. (15) and work in the opposing limit, $(\sigma_1+\sigma_2)>>\Gamma$, so the approximation $\arctan x\sim\frac{\pi}{2}-\frac{1}{x}$ when $x\to\infty$ can be used, yielding

$$\Gamma_{SBBSwf}^{\max}=\frac{\pi a_0^2\omega_{pi}^2}{16c_Sk_0}\frac{k_0+\sigma_2}{\sigma_1+\sigma_2}\frac{1}{1+\frac{a_0^2\omega_{pi}^2}{16c_Sk_0}\frac{k_0+\sigma_2}{(\sigma_1+\sigma_2)^2}}. \quad (17)$$

The corresponding saturation value for large bandwidth is

$$\Gamma_{SBBSwf}^{\max,sat}=\frac{\pi a_0^2\omega_{pi}^2}{16c_Sk_0}. \quad (18)$$

We also recall the obtained limit for the monochromatic case (16), now expressed in a simpler way,

$$\Gamma_{SBBSwf}^{pw,\max}=\frac{a_0\omega_{pi}}{2\sqrt{c_S}}. \quad (19)$$

2. Strong field limit

We now consider the strong field limit, i.e., we assume that $|\omega_L|>>k_Lc_S$.

We work under the underdense limit as in the weak field case, so that the range of unstable wave numbers still holds and we use $k_L\approx 2(k_0+\sigma_2)$ as the wave number for maximum growth, which means that k_L is still of the order of k_0. We also neglect $|\omega_L|$ when compared to k_0, which establishes the scale $k_Lc_S<<|\omega_L|<<k_L\approx k_0$, consistent with $c_S<<1$. This means that we are not neglecting the magnitude of the imaginary part of ω_L when compared to its real part.

We now expand $\omega_L=\alpha+i\beta$, with real α and β, so that the dispersion relation yields (as detailed in the thesis document [27])

$$\omega_L=\left(\frac{k_La_0^2\omega_{pi}^2}{2}\right)^{1/3}\left(\frac{1}{2}+\frac{\sqrt{3}}{2}i\right), \quad (20)$$

which is, once more, the result presented in [1] with the usual polarization considerations. The maximum growth rate in the strong field limit is then

$$\Gamma_{SBBSsf}^{pw,\max}=\frac{\sqrt{3}}{2}\left(\frac{k_La_0^2\omega_{pi}^2}{2}\right)^{1/3}. \quad (21)$$

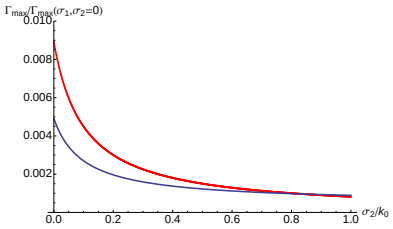

FIG. 1: Maximum growth rate of SBBS as a function of bandwidth - $a_0 = 0.1$, $k_0 = 80.0$, $\sigma_1 = 0.1k_0$, $c_S = 0.01$, $\omega_{pi} = 0.1$. Red line - numerical solution; blue line - analytical limit for $\Gamma << (\sigma_1 + \sigma_2)$ of Eq. (17)

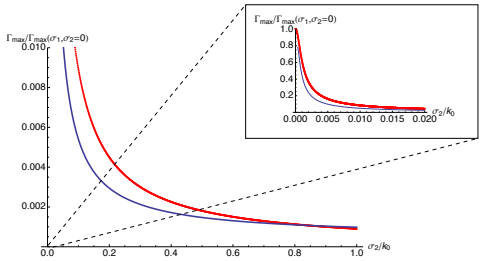

FIG. 2: Maximum growth rate of SBBS as a function of bandwidth - $a_0 = 0.1$, $k_0 = 80.0$, $\sigma_1 \approx 0$, $c_S = 0.01$, $\omega_{pi} = 0.1$. Red line - numerical solution; blue line - analytical limit for $\Gamma << (\sigma_1 + \sigma_2)$

D. Numerical solution of the complete dispersion relation

The numerical solution of the complete dispersion relation illustrates the evolution of the strength of the instability as a function of, not only the bandwidth, but also the wave number of the scattered wave itself.

In Fig. 1 we show the maximum growth rate of the Brillouin instability as a function of the bandwidth parameter, σ_2, as σ_1 was kept fixed. As expected, Eq. (17) is a good approximation to the complete solution only when we are dealing with large bandwidths. The difference between the approximate and the numerical solutions increases as bandwidth (σ_2) decreases. As σ_2 approaches k_0, the results start to agree and Eq. (17) can be used. As we approach the monochromatic limit, only the numerical solution should be considered, as the choice of $\sigma_1 = 0.1k_0$ still accounts for a considerable difference between $\Gamma_{\max}(\sigma_2 = 0)$ and the maximum growth rate in the monochromatic limit, $\Gamma_{\max}(\sigma_1, \sigma_2 = 0)$, expressed by Eq. (19). It is clear that a bandwidth as small as 10% can still cause a reduction of the growth rate of the instability by a factor of more than 100, which is quite significant.

Fig. 2 shows the same results for the case of $\sigma_2 \approx 0$. As in the previous case, the approximation of Eq. (17) agrees with the numerical solution as σ_2 approaches k_0. The monochromatic limit of Eq. (19) can also be confirmed at the origin of the plot, as expected.

We now study the behavior of the growth rate of the instability as a function of the wave number of the scattered wave. In Fig. 3, we plot the growth rate for a set of bandwidths and express it as a function of the wave number of the instability. We observe a very good agreement with the range of unstable wave numbers predicted by Eq. (12). The lower limit does not depend on σ_2 and

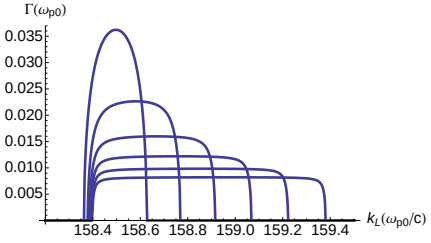

FIG. 3: Growth rate of SBBS as a function of the wave number of the scattered wave for different bandwidths of the water-bag (from the left to the right: $\sigma_2 = 0.1k_0, 0.2k_0, 0.3k_0, 0.4k_0, 0.5k_0, 0.6k_0$, with $a_0 = 0.1$, $k_0 = 80.0$, $\sigma_1 \approx 0$, $c_S = 0.01$ and $\omega_{pi} = 0.1$)

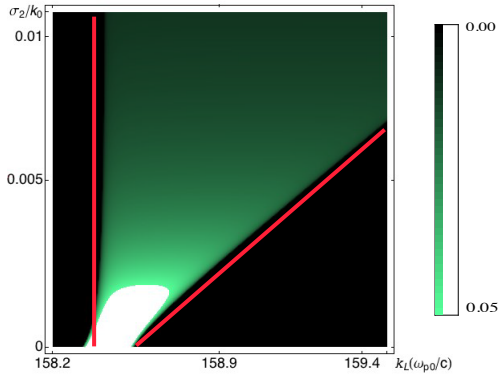

FIG. 4: Growth rate of SBBS as a function of the wave number of the scattered wave and the bandwidth of the water-bag: $a_0 = 0.1$, $k_0 = 80.0$, $\sigma_1 \approx 0$, $c_S = 0.01$, $\omega_{pi} = 0.1$ (2D representation). The red lines illustrate the theoretical range of unstable wave numbers

remains fixed as we increase bandwidth; as for the upper bound, it linearly grows as we increase the value of σ_2.

We should also note that the flat structure observed indicates that the magnitude of the growth rate is within the same order for the full range of unstable wave numbers, meaning that the instability can grow on a wide range of wave numbers and lead to significant phenomena of turbulence. This is valid for relatively small bandwidths, as it is clear for $\sigma_2 > 0.1k_0$.

In Fig. 4, we provide a two-dimensional (2D) representation of the variation of the growth rate of SBBS as a continuous function of both the bandwidth of the pump and the instability wave number, which allows for a global picture of the instability. As expected, we observe a strong dependence of the instability on the bandwidth of the radiation used as a driver. For a bandwidth of just 1% in k_0, the instability is already reduced to 10% of the plane wave limit, which justifies the use of bandwidth as a means of significantly reducing the strength of the instability.

For fixed k_0, a_0 and σ_1, the growth rate for SBBS scales with $\propto 1/\sigma_2$, similarly to other distribution functions (e.g., asymmetric Lorentzian or Gaussian distribution of photons [16]). Both the wave number for maximum growth and the upper bound of the unstable wave numbers domain depend linearly on σ_2.

III. COMPARISON WITH PREVIOUS MODELS FOR STIMULATED BRILLOUIN SCATTERING

Having performed a detailed comparison of the results provided by Generalized Photon Kinetics with classical references, such as [1], that focused on the monochromatic limit of our general dispersion relation, we now focus on more recent models for Stimulated Brillouin Scattering including bandwidth effects of the pump wave. In particular, we compare our results with [21], [22], developed under the same physical assumptions but dealing essentially with distinct geometries for the problem. In order to further explore the validity and wide applicability of our model, we focus on the model from Ref. [21], whose conditions differ the most from the regime we have considered so far (backscattering).

A. Forward Stimulated Brillouin Scattering (FSBS)

The first analytic theory of broadband Forward Stimulated Brillouin Scattering [21] was developed in the regime of small coherence time of the laser beam. In particular, Lushnikov and Rose (LR) focused on a collective regime of the FSBS instability which couples the beam to transversely propagating low frequency ion acoustic waves.

With the definition of three dimensionless parameters, ν, the Landau damping coefficient, $\tilde{I}_0 \equiv \left(\frac{k_0}{k_m}\right)^2 \frac{n_e}{n_c}\frac{I_0}{\nu}$ and $\tilde{T}_c = k_m c_S T_C$ (with k_m the wave number spread of the pump wave as in the idealized *top hat* model of NIF optics, $I_0 \equiv \langle |E|^2 \rangle$ and T_c the coherence time of the laser) and while looking for solutions of the form $\delta\rho \sim e^{\lambda z} e^{i(\mathbf{k}.\mathbf{x}-\omega t)}$, for real $\mathbf{k}$ and ω but imaginary λ, LR obtain an explicit expression for the normalized $\tilde{\lambda} \equiv k_0/k_m^2 \lambda$ parameter.

The Lushnnikov-Rose model provides an explicit expression for the instability growth rate (which corresponds to the real part of the λ parameter $\equiv \Gamma_{LR}$). We now derive an equivalent result via GPK.

B. Generalized Photon Kinetics applied to Forward Stimulated Brillouin Scattering

We recall that the form of the general dispersion relation, Eq. (6) derived in the previous section, quickly allows the translation of the problem to the GPK formalism language

$$1 = \frac{\omega_{pi}^2}{4} \frac{\mathbf{k}_L^2}{\omega_L^2 - c_S^2 \mathbf{k}_L^2 + 2i\nu\omega_L |\mathbf{k}_L| c_S} \int \rho_0(\mathbf{k}) \left(\frac{1}{D^+(\mathbf{k})} + \frac{1}{D^-(\mathbf{k})} \right) d\mathbf{k}, \tag{22}$$

where we have already accounted for the linear polarization of the pump wave.

We choose a pump wave which propagates in the z direction with k_0 wave number and exhibits a wave number spread in the transverse direction, x, in the form of a water-bag, so that $\rho_0(\mathbf{k}) = \frac{a_0^2}{k_m} [\theta(k_x) - \theta(k_x - k_m)]\, \delta(k_y)\delta(k_z - k_0)$.

Finally, we seek growth of the instability in the longitudinal direction and oscillation in the transverse direction so that the wave vector for the instability can be written as $\mathbf{k}_L = k_L \mathbf{e}_x + i\lambda \mathbf{e}_z$, with real k_L but allowing for the simultaneous development of a real and imaginary part in λ. With this expression for $\mathbf{k}_L$, the vector potential evolves as $e^{i(\omega_L t - \mathbf{k}_L.\mathbf{r})} = e^{\lambda z} e^{i(\omega_L t - k_L x)}$, and therefore a positive Re(λ) corresponds to condition for the instability to occur. Note that the choice $\mathbf{k}_L = k_L \mathbf{e}_x + i\lambda \mathbf{e}_z$ implies that $\mathbf{k}_L^2 = k_L^2 - \lambda^2$ and $|\mathbf{k}_L| = \sqrt{k_L^2 + |\lambda|^2}$

This complete dispersion relation can be solved numerically for a given k_L and a range of ω_L. We then seek:

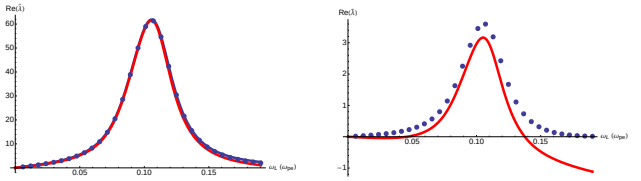

(a)$k_m = 1\%k_0$ + monochromatic limit (b)$k_m = 4\%k_0$

FIG. 5: Normalized instability growth rate for a scenario without static response: $k_0 = 80.0(\omega_{pe}/c), a_0 = 1.0(m_e c^2/e), \omega_{pi} = 0.1(\omega_{pe}), c_S = 0.01(c), \nu = 0.15, k_L = 11.19(\omega_{pe}/c)$. Blue dots - GPK dispersion relation numerical solution; red lines - LR model explicit expression evaluation; blue line - monochromatic limit ($k_m = 0$)

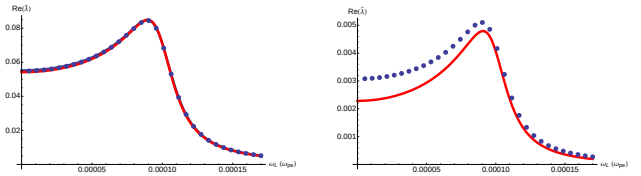

(a)$k_m = 1\%k_0$ + monochromatic limit (b)$k_m = 4\%k_0$

FIG. 6: Normalized instability growth rate for a scenario with static response: $k_0 = 80.0(\omega_{pe}/c), a_0 = 1.0(m_e c^2/e), \omega_{pi} = 0.1(\omega_{pe}), c_S = 0.01(c), \nu = 0.15, k_L = 0.01(\omega_{pe}/c)$. Blue dots - GPK dispersion relation numerical solution; red lines - LR model explicit expression evaluation; blue line - monochromatic limit ($k_m = 0$)

$$\tilde{\Gamma}_{GPK} \equiv \frac{k_0}{k_m^2} \mathrm{Re}(\lambda) \equiv \frac{k_0}{k_m^2} F'_{GPK}(k_L, \omega_L) \equiv F_{GPK}(k_L, \omega_L), \tag{23}$$

where F'_{GPK} represents the numerical solution for Re(λ) of Eq. (22). Details of this calculation are presented in [27].

C. Comparison between models

In the following comparison we choose a set of parameters that provides a suitable scenario for SBS growth. In particular, the perturbation wave number corresponds to that of maximum growth rate. We also study the range of unstable frequencies around the resonance condition of $\omega_L = k_L c_S$, so that the expected resonance peak is clear. For this configuration and choice of parameters, we observe no static response from the plasma ions, which means that for $\omega_L = 0$ no instability develops. This together with the analytical result for $\tilde{\Gamma}_{LR}$, the numerical solution for $\tilde{\Gamma}_{GPK} = F_{GPK}(k_L, \omega_L)$, and the classical/monochromatic limit of the dispersion relation, obtained in the limit $k_m \to 0$, are shown in Fig. 5.

In order to further analyze the validity and robustness of the GPK dispersion relation, we select a different range of unstable wave numbers to work, in particular, one which would stimulate a static response of the instability ($\tilde{\Gamma}(\omega_L = 0) \neq 0$). Although this corresponds to a mode with smaller growth rates, the comparison may still be performed. The results are presented in Fig. 6.

Bandwidth is currently a limitation for both models: in the Lushnikov-Rose model, the validity of the equation that defines the driving term is restricted to the condition $F^2 >> 1 \Rightarrow k_m \approx k_0/2F << k_0$, where F is the optic f number of the lens; in the

dispersion relation solution of our GPK we have assumed small spread of transverse wave numbers, which means that $k_x << k_0$. This is equivalent to the assumption $k_m << k_0$, since k_x has a range which corresponds to the whole $[0, k_m]$ interval.

The difference between the previous solution and the solution of the complete dispersion relation (obtained relaxing the small transverse spread assumption),

$$1 = \frac{a_0^2\omega_{pi}^2}{4k_m}\frac{k_L^2-\lambda^2}{\omega_L^2 - c_S^2k_L^2 + c_S^2\lambda^2 + 2i\nu\omega_L\sqrt{k_L^2+|\lambda|^2}c_S}\times$$

$$\times\int_0^{k_m}\frac{1}{D^+(k_x,k_L,\lambda,\omega_L)} + \frac{1}{D^-(k_x,k_L,\lambda,\omega_L)}dk_x, \quad (24)$$

with $D^{\pm}(k_x,k_L,\lambda,\omega_L) \equiv \omega_L^2 - k_L^2 + \lambda^2 \pm 2\sqrt{\omega_0^2+k_x^2}\omega_L \mp 2(k_xk_L + i\lambda k_0)$, and $\omega_0 \equiv \sqrt{1+k_0^2}$, is negligible, so our approximation is valid for the chosen parameters.

The GPK formalism deals with the two-mode problem contained in the full Klein-Gordon or wave equation, completely describing the dynamics of not only the forward propagating radiation but also of its backscattered component and their beating. The driving term in the Lushnikov-Rose model is clearly a one-mode approach to the physics of the problem. This may account for the detected quantitative differences as we increase the bandwidth of the pump wave.

IV. SIMULATIONS OF BROADBAND DRIVEN INSTABILITIES

A. First simulations of monochromatic driven instabilities

The first detailed PIC simulation studies of stimulated Brillouin scattering in an underdense plasma [28]-[31] already included the modeling of collisionless nonlinear saturation mechanisms and showed their critical dependence on the plasma composition. More recently, C. Riconda *et al.* focused on the role of electron kinetic effects in the nonlinear evolution of a driven ion-acoustic wave [31]-[32].

The computational setup for our PIC simulations can be briefly described as follows. We select a plasma density above the quarter-critical density of $n_e = 0.3n_c(> 0.25n_c)$, in order to avoid the excitation of Raman Backscattering. The driver is injected through the Antenna feature of OSIRIS 2.0 while avoiding a steep envelope, which prevents the incident light wave from instantaneously pushing away all the plasma, as well as the eventual onset of Raman Forward Scattering processes. The temperature of each species is set to $T_e = 500eV$ and $T_i = 10eV$, thus allowing for Landau damping to be neglected. This corresponds to a characteristic sound velocity for the initially thermal plasma of about $c_S = 7\times10^{-7}$, in normalized units. The electron quiver velocity is $v_{osc} \equiv eE/m_e\omega_0 = 0.085$, which corresponds to an intensity of $I = 1\times10^{16}W/cm^2$ for a laser wavelength of $\lambda_0 = 1\mu m$. The ions are modeled as protons, so $M \approx 1836$. The plasma is composed of two ramps ($1\lambda_0$ each) and a plateau of length $38\lambda_0$, completely separated by large vacuum regions ($40\lambda_0$ on both sides) such that the boundary conditions for the particles do not influence the interaction physics for the duration of the simulation. We choose a time step of about $dt = (5\times10^{-2})\omega_0^{-1}$, while working with more than 5000 cells and 100 particles per cell in a 1D simulation. This choice of parameters corresponds to one of the theoretical limits we explored in section II: the strong coupling limit, as we have $4k_0C_S\omega_0/\omega_{pe}^2 \approx 0.01 \ll (v_{osc}/v_e) = 7.2$, where $v_e = \sqrt{\theta_e/m_e}$ is the electron thermal velocity.

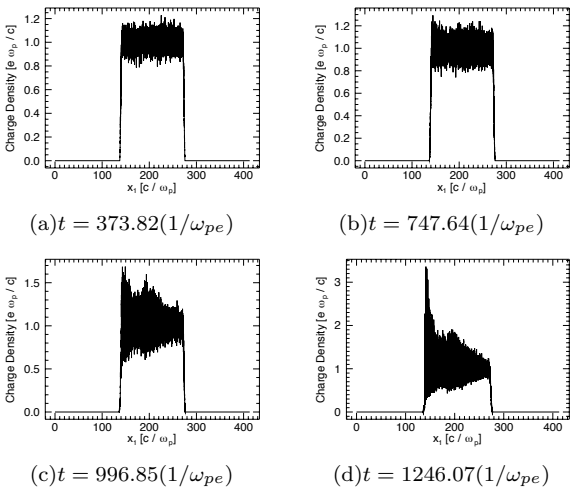

(a)$t = 373.82(1/\omega_{pe})$ (b)$t = 747.64(1/\omega_{pe})$

(c)$t = 996.85(1/\omega_{pe})$ (d)$t = 1246.07(1/\omega_{pe})$

FIG. 7: Evolution in time of the ion density during the linear ((a) and (b)) and nonlinear ((c) and (d)) growth phase of SBS instability. The ion density ripple is created from noise and is enhanced by the ponderomotive force, as the incident field couples with ion plasma waves

The time evolution of the ion density is suitable for the detection of the growth of Stimulated Brillouin Scattering processes. In fact, we expect a modulation of this quantity in space, according to the wave number for maximum growth rate predicted in section II. The ripple in the ion density, despite being created by random noise in the species density, is the perturbation responsible for the coupling of the incident field to a scattered light wave which will, in turn, enhance the ion density perturbation through the ponderomotive force. In Fig. 7, we present the evolution of the ions profile for some selected time steps. The correspondent Fourier spectra are presented in Fig. 8.

We theoretically predicted that the maximum growth would correspond to the backscattering regime of the instability. This can be easily verified, as the peak in the Fourier spectrum occurs for $k_L \approx 2k_0$, the condition for backscattering. This is also clear if we plot the electron density or the component of the electric field which corresponds to the scattered light wave, as these quantities should all grow with the same characteristic frequency and wave number.

Plotting the peak value of the Fourier spectrum against time, during the linear growth phase of the process, allows for an estimation of the instability growth rate, as presented in figure 9.

As expected and highlighted in Ref. [32], the instability quickly saturates once the density cavity is formed. This not only suppresses the fundamental wave number growth in the Fourier spectrum, but also the growth of its harmonics, which appear for $k_L = 4k_0$ and $k_L = 6k_0$. These harmonics are clearly sharper than the fundamental component and grow with significant magnitude, but do not seem to affect the growth rate predictions. If the growth rate estimate is entirely performed in the linear growth phase, thus avoiding the effects of saturation, the agreement with the predictions of GPK is perfect, as we recover

$$\Gamma_{SBBSsf}^{pw,\max} = \frac{\sqrt{3}}{2}\left(\frac{k_La_0^2\omega_{pi}^2}{2}\right)^{1/3}, \quad (25)$$

the result from section II.

We have reached qualitative and quantitative agreement between the predictions of GPK and the estimates from PIC simulations of monochromatic driven instabilities in OSIRIS 2.0. We now focus on the new feature of the simulation code which corresponds, also

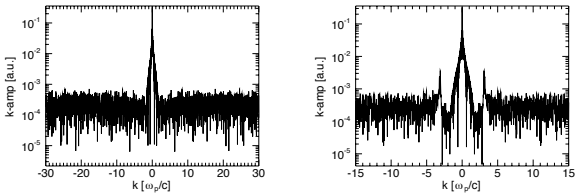

(a)$t = 373.82(1/\omega_{pe})$ (b)$t = 747.64(1/\omega_{pe})$

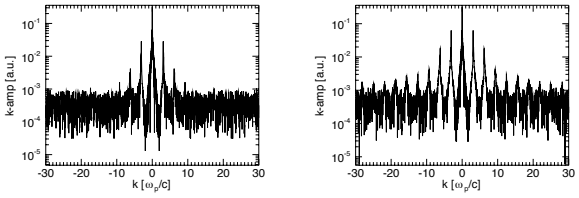

(c)$t = 996.85(1/\omega_{pe})$ (d)$t = 1246.07(1/\omega_{pe})$

FIG. 8: Evolution in time of the Fourier spectrum of the ion density during the linear ((a) and (b)) and nonlinear ((c) and (d)) growth phase of SBS instability. The nonlinear phase corresponds to the growth of harmonics and coincides with the ion bunching on the left side of the plasma, as depicted in Fig. 7

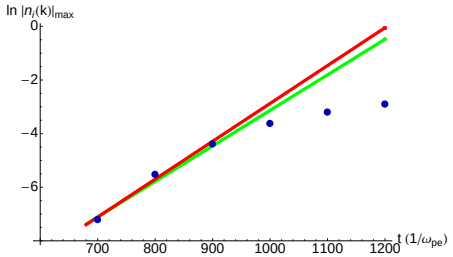

FIG. 9: SBS instability growth rate estimate. Blue dots - simulation points; red line - linear growth phase simulation fit; green line - theoretical prediction. The growth of the harmonics represent the end of the linear growth phase, right before saturation takes place [31], [32]

in a theoretical point of view, to the novelty of our model: a pump wave with finite bandwidth.

B. Bandwidth implementation in OSIRIS 2.0

The main objective of this section is to provide an implementation of a broadband pump wave which, in a PIC simulation scenario, would be consistent with the one-dimensional zero-order photon distribution function we assumed in section II,

$$\rho_0(k) = \frac{a_0^2}{\sigma_1 + \sigma_2}[\Theta(k - k_0 + \sigma_1) - \Theta(k - k_0 - \sigma_2)] \tag{26}$$

This means that the spectra of the vector potential and the electric field of the incident laser will also have a water-bag profile.

We begin with a well-known source of noise whose statistical properties we know beforehand: the white noise. White noise corresponds to an arbitrary spatial/temporal profile (as pictured in Fig. 10(a)) with a gaussian probability distribution function. In the k-spectrum, this noise sample corresponds to a profile which

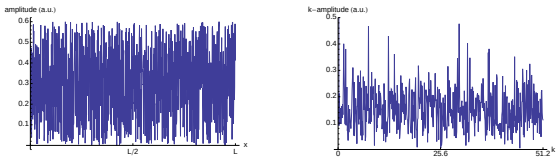

(a)Spatial profile (b)Fourier spectrum

FIG. 10: Sample of white noise, with wave numbers covering the whole non-redundant Nyquist range in arbitrary units

has, in average, a constant amplitude for the whole infinite range of wave numbers. The example depicted in Fig. 10(b) could be averaged over a significant number of samples (as we will later show) to provide an infinitely wide water-bag in k-space.

We still need to filter our noise sample so it will acquire a finite bandwidth around a specified wave number. In the Fourier space, such operation is trivial, as the filter itself is a water-bag centered in k_0 with a $(\sigma_1 + \sigma_2)$ wave number bandwidth. The filtering process in k-space corresponds to the product of the Fourier spectra of the signals, capturing the white noise profile in the range $[k_0 - \sigma_1, k_0 + \sigma_2]$. The equivalent process in the x-space should now be found, as we are interested, in the end, in the spatial profile of the noise sample, and the process of Fourier transforming is just a theoretical tool to make the analysis easier but still computationally heavy.

In real space, the equivalent operation to the product of Fourier spectra is the well-known convolution of two functions. If we have two signals described in the x-space, $A(x)$ and $B(x)$, with $\bar{A}(k) = \mathcal{F}(A)$ and $\bar{B}(k) = \mathcal{F}(B)$ their respective Fourier transforms, then $\mathcal{F}^{-1}(\bar{A}(k) \times \bar{B}(k)) = (A * B)(x)$, where the $*$ convolution operation is defined in the usual way,

$$(A * B)(x) \equiv \int_{-\infty}^{+\infty} A(\delta)B(x - \delta)d\delta \tag{27}$$

All the analysis and signal synthesis can be performed in the x-space, as long as we have the spatial profile of the filter. From a computational point of view, we also need to work with a finite series representation of the white noise sample. The filter itself can be modeled as a sinc function in x-space

$$\text{sinc}(2Bx) \equiv \begin{cases} \frac{\sin(2Bx)}{2Bx} & , \ x \neq 0 \\ 1 & , \ x = 0 \end{cases}$$

which corresponds, in k-space, to a zero-centered filter with total bandwidth $2B$. If this band-pass is multiplied by a regular sine function, it becomes centered in a desired wave number, according to the argument of that sine function. The complete filter has a spatial profile (Fig. 11) which can be described as

$$\text{filter}(x) = \sin(k_0 x) \times \text{sinc}(2Bx) \tag{28}$$

which provides a water-bag-like filter for the range $[k_0 - B, k_0 + B]$ in k-space.

One single sample of filtered white noise can then be written as

$$\text{pump}(x) = p_0 \times (\text{filter} * \text{white noise})(x) \tag{29}$$

where white noise(x) represents a set of randomly generated values with a gaussian probability distribution function. In Fig. 12(a), we present a sample of such a signal in real space, and in Fig. 12(b) its respective sprectrum.

We performed a robust average of this process over more than 10,000 samples of filtered white noise, and the result is presented in Fig. 13. The desired Fourier profile has then been accomplished: a water-bag in the range $[k_0 - B, k_0 + B]$. The translation to the

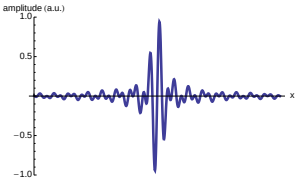

FIG. 11: Spatial profile of a filter for the $[k_0 - B, k_0 + B]$ range

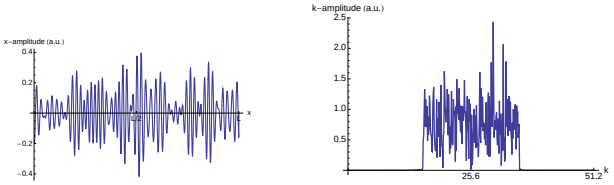

(a)Spatial profile (b)Fourier spectrum

FIG. 12: Sample of filtered white noise. In the spectrum, wave numbers cover the whole non-redundant Nyquist range in arbitrary units

$[k_0 - \sigma_1, k_0 + \sigma_2]$ range is quite trivial, since $[\bar{k}_0 - B, \bar{k}_0 + B]$ and $[k_0 - \sigma_1, k_0 + \sigma_2]$ represent the same interval if $\bar{k}_0 = k_0 + \frac{\sigma_2 - \sigma_1}{2}$ and $B = \frac{\sigma_1 + \sigma_2}{2}$. The amplitude of the pump wave can be manipulated by multiplying the convolution signal by a desired constant p_0, already present in (29).

This procedure can now be readily discretized and implemented in the PIC code, OSIRIS 2.0.

C. Simulations of broadband driven parametric instabilities

We study the qualitative and quantitative behavior of the growth rate and unstable domain of SBS driven by a broadband pump wave. Theoretical estimates of the scattering process properties (see section II) predicted a significant suppression of the instability even for small bandwidth values. In particular, it is possible to reduce the strength of the instability by a factor of more than 10 with a bandwidth as small as 1% of the incident wave number. The growth rates of SBS are not only function of the pump's bandwidth, but they also exhibit a clear dependence on the intensity (a_0) and

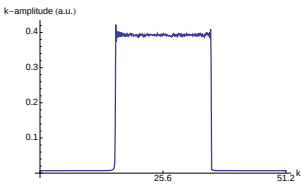

FIG. 13: Averaged spectrum of filtered white noise over 10,000 samples

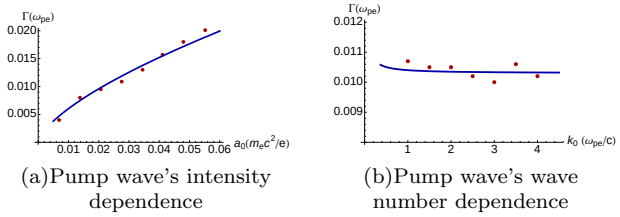

(a)Pump wave's intensity dependence (b)Pump wave's wave number dependence

FIG. 14: Evolution of the SBBS growth rate with the pump wave's parameters for a fixed bandwidth (10% of k_0). Blue line - numerical solution of the complete dispersion relation of GPK; red dots - estimates from PIC simulations

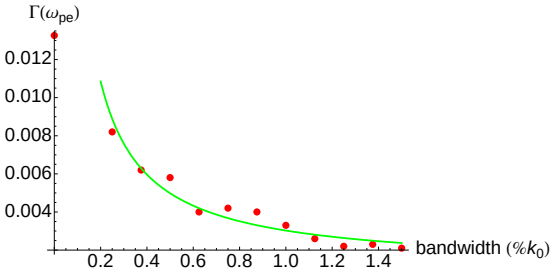

FIG. 15: Evolution of the SBBS growth rate with the pump wave's bandwidth. Green line - GPK theoretical growth rate as a numerical solution of the complete dispersion relation; red dots for $\sigma \neq 0$ - growth rate estimates from PIC simulations; red dot for $\sigma = 0$ - monochromatic limit (theory and simulation)

wave number (k_0) of the incident light wave. Classical theories that modeled SBS processes [1] explicitly included these effects (Eqs. (19) and (21)), but as bandwidth is increased it is not reasonable to assume that the same kind of functional dependences on these parameters will be preserved. This can be seen in the particular case of the weak field limit, for which we derived an analytical expression for the growth rate as a function of the pump wave's parameters, Eq. (17).

We worked with a fixed but still significant bandwidth value (10% of k_0) and obtained estimates of the growth rate of the instability as the intensity (Fig. 14(a)) and wave number (Fig. 14(b)) of the pump wave were manipulated. The agreement with the theoretical estimates for the evolution of the strength of the instability as a function of the amplitude and wave number of the incident field is extremely good, supporting the bandwidth implementation in OSIRIS 2.0.

In Fig. 15, we simultaneously plot the growth rate estimates for a pump plane wave (obtained in section IV A) and the results obtained with the new bandwidth implementation of the PIC code. We also include the numerical solution of the complete dispersion of GPK, which roughly predicts a suppression of the instability with $\propto 1/(\sigma_1 + \sigma_2)$, similarly to Eq. (17).

V. CONCLUSIONS

A general dispersion relation for stimulated Brillouin scattering, driven by a partially coherent pump field, was derived, using a result [16] which is formally equivalent to the coupling of the full wave equation with the plasma fluid equations. After retrieving the monochromatic limit of the equation, we used a one-dimensional water-bag profile for the incident field to model broadband effects.

The analysis revealed a growth rate dependance on the coherence width σ of the radiation field which scales with $1/\sigma$ for backscattering. In addition, a numerical estimate of the growth rate of the instability was obtained as a function of the intensity of the incident field and the wave number of the scattered wave, confirming the theoretical predictions for the domain of unstable wave numbers.

Good agreement (perfect for the monochromatic limit) was found between our results and those provided by a previous model for broadband SBS, as qualitatively distinct regimes were considered.

We have illustrated and compared the results of previous sections with estimates from parametric instabilities PIC simulations. We have initially focused on standard simulations whose scattering processes were driven by monochromatic pump waves, thus establishing a suitable set of parameters for the onset of the instability. The classical growth rate and unstable domain estimates, consistent with the GPK predictions, have also been supported by the presented simulations, which we have carefully described. A numerical procedure for the broadening of the pump wave has been presented in detail and readily implemented in the standard PIC code, allowing for an extensive study of the sensitivity of the scattering process to the driver's properties, in particular, its bandwidth. An excellent agreement has also been found as these results where plotted against the numerical solution of the complete dispersion relation of GPK for the process.

From the work presented here, we draw two main conclusions. As far as Stimulated Brillouin Scattering is concerned, one of the features of the laser that is usually taken as a nonideality, its partial incoherence, is actually an effective way to suppress the undesirable effects of the associated instability. With the present study, Generalized Photon Kinetics establishes itself as an adequate model to capture the full dynamics of the propagation of an electromagnetic wave in a dispersive nonlinear medium. Our description of Brillouin scattering processes is valid for all angles, all intensities and a spatially stationary pump wave with arbitrary statistics, providing an important addition to the previous study of Raman scattering processes developed by Jorge Santos *et al.* [16].

Some aspects to be addressed in future works include a spatio-temporal description of the instability (convective and absolute regimes), the measurement of broadband effects on stimulated Raman scattering and modulational instabilities, with analytical and numerical approaches, as well as a coupling with the statistical theory for plasma fluctuations. It should also be noted that the PIC-oriented bandwidth implementation for the pump wave as been thoroughly tested, so the generalization of this work to self-focusing and stimulated Raman scattering should be straightforward.

[1] William L. Kruer, *The Physics of Laser Plasma Interactions* (Addison-Wesley, 1988).

[2] C. Thompson, R. D. Blandford, C.R. Evans, E.S. Phinney, *Physical Processes in Eclipsing Pulsars: Eclipse Mechanisms and Diagnostics*, The Astrophysical Journal **422**, 304 (1994).

[3] T. M. Antonsen and P. Mora, *Self-focusing and Raman scattering of laser pulses in tenuous plasmas*, Physics of Fluids B **5**, 1440 (1993)

[4] P. Mora and T. M. Antonsen, *Kinetic modeling of intense, short laser pulses propagating in tenuous plasmas*, Physics of Plasmas **4**, 217 (1997)

[5] B. Hall, M. Lisak, D. Anderson, R. Fedele, and V. E. Semenov, *Statistical theory for incoherent light propagation in nonlinear media*, Physical Review E **65**, 035602(R) (2002).

[6] D. Anderson, L. Helczynski-Wolf, M. Lisak, and V. E. Semenov, *Features of modulational instability of partially coherent light: Importance of the incoherence spectrum*, Physical Review E **69**, 025601 (2004).

[7] D. Anderson, L. Helczynsci-Wolf, M. Lisak and V. E. Semenov, *Transverse modulational instability of partially incoherent soliton stripes*, Physical Review E **70**, 026603 (2004).

[8] E. J. Valeo and C. R. Oberman, *Model of Parametric Excitation by an Imperfect Pump*, Physical Review Letters **30**, 1035 (1973).

[9] J. J. Thomson, W. L. Kruer, S. E. Bodner, and J. S. DeGroot, *Parametric instability thresholds and their control*, Physics of Fluids **17**, 849 (1974).

[10] J. J. Thomson and Jack I. Karush, *Effects of finite-bandwidth driver on the parametric instability*, Physics of Fluids **17**, 1608 (1974).

[11] G. Laval, R. Pellat, and D. Pesme, *Absolute Parametric Excitation by an Imperfect Pump or by Turbulence in an Inhomogeneous Plasma*, Physical Review Letters **36**, 192 (1976).

[12] G. Laval, R. Pellat, D. Pesme, A. Ramani, Marshall N. Rosenbluth, and E. A. Williams, *Parametric instabilities in the presence of space-time random fluctuations*, Physics of Fluids **20**, 2049 (1977).

[13] J. J. Thomson, *Stimulated Raman scatter in laser fusion target chambers*, Physics of Fluids **21**, 2082 (1978).

[14] K. Mizuno and J. S. DeGroot, *Measurements of Finite-Bandwidth Effects on a Parametric Instability*, Physical Review Letters **39**, 608 (1977).

[15] J. P. Santos and L. O. Silva, *Wigner-Moyal description of free variable mass Klein-Gordon fields*, Journal of Mathematical Physics **46**, 102901 (2005).

[16] J. E. Santos, L. O. Silva, and R. Bingham, *White-Light Parametric Instabilities in Plasmas*, Physical Review Letters **98**, 235001 (2007).

[17] M. J. Bastiaans, *Wigner Distribution function and its application to first order optics*, Journal of the Optical Society of America **69**, 12 (1979).

[18] M. J. Bastiaans, *The Wigner distribution function of partially coherent light*, Optica Acta **28**, 9 1215 (1981)

[19] M. J. Bastiaans, *Application of the Wigner disctribution function to partially coherent light*, Journal of the Optical Society of America **3**, 8 (1986).

[20] T. A. C. M. Claasen and W. F. G. Mecklenbrauker, *The Wigner distribution - A tool for time-frequency signal analysis. Part III: Relations with other time-frequency signal transformations*, Philips Journal of Research **35**, 372-389 (1980).

[21] Pavel M. Lushnikov and Harvey A. Rose, *Instability Versus Equilibrium Propagation of a Laser Beam in Plasma*, Physical Review Letters **92**, 255003 (2004).

[22] Pavel M. Lushnikov and Harvey A. Rose, *Collective stimulated Brillouin backscatter*, arXiv:0710.0634v1 (2007).

[23] C. D. Decker, W. B. Mori, T. Katsouleas, and D. E. Hinkel, *Spatial temporal theory of Raman forward scattering*, Physics of Plasmas **3**, 1360 (1996).

[24] C. D. Decker, W. B. Mori, K.-C. Tzeng, and T. Katsouleas, *The evolution of ultra-intense, short-pulse lasers in underdense plasmas*, Physics of Plasmas **3**, 2047 (1996).

[25] P. K. Kaw, G. Schmidt, and T. Wilcox, *Filamentation and trapping of electromagnetic radiation in plasmas*, Physics of Fluids **16**, 1522 (1973).

[26] A. J. Schmitt, *The effects of optical smoothing techniques on filamentation in laser plasmas*, Physics of Fluids **31**, 3079 (1988).

[27] B. Brandão, *White Light Parametric Instabilities in Plasmas*, MSc Thesis document, September 2008.

[28] W. L. Kruer, E. J. Valeo, and K. G. Estabrook, *Limitation of Brilluin Scattering in Plasmas*, Physical Review Letters **35**, 1076 (1975).

[29] H. A. Baldis, P. E. Young, R. P. Drake, W. L. Kruer, K. Estabrook, E. A. Williams, and T. W. Johnston, *Competition*

between the Stimulated Raman and Brillouin Scattering Instabilities in $0.35 - \mu m$ *Irradiated CH Foil Targets*, Physical Review Letters **62**, 2829 (1989).

[30] S. C. Wilks, W. L. Kruer, J. Denavit, K. Estabrook, D. E. Hinkel, D. Kalantar, A. B. Langdon, B. MacGowan, D. S. Montgomery, and E. A. Williams, *Nonlinear Theory and Simulations of Stimulated Brilouin Backscatter in Multispecies Plasmas*, Physical Review Letters **74**, 5048 (1995).

[31] C. Riconda, A. Heron, D. Pesme, S. Hüller, V. T. Tikhonchuk, and F. Detering, *Electron Kinetics Effects in the Nonlinear Evolution of a Driven Ion-Acoustic Wave*, Physical Review Letters **94**, 055003 (2005).

[32] S. Weber, C. Riconda, and V. T. Tikhonchuk, *Low-Level Saturation of Brillouin Backscattering due to Cavity Formation in High-Intensity Laser-Plasma Interaction*, Physical Review Letters **94**, 055005 (2005).